Revision 3

Low pressure crystallization of a volatile-rich lunar basalt: a means for producing local anorthosites?

Nicholas J. DiFrancesco[1,*], Hanna Nekvasil[1], Donald H. Lindsely[1], and G. Ustunisik[2]

[1]Stony Brook University, Department of Geosciences, Earth and Space Science Building, Stony Brook, NY 11794.

[2]American Museum of Natural History, Department of Earth and Planetary Sciences, New York, NY 10024.

*Present Address: Department of Geosciences, Stony Brook University, Stony Brook, NY 11794. E-mail: Nicholas.Difrancesco@stonybrook.edu.

Abstract

The presence of anorthosite in the lunar highlands containing plagioclase that is compositionally less calcic than plagioclase in the ferroan anorthosites cannot be readily explained by the current lunar paradigm in which lunar anorthosite was produced as a floatation cumulate in the lunar magma ocean. Phase equilibrium experiments were conducted to investigate whether such anorthosite could arise locally from crystallization of aluminous magma at shallow levels within the lunar crust. The experiments were conducted on a synthetic analog of Cl-, F-, and S-bearing aluminous highland basalt 14053 at pressures of approximately 1 bar and f_{O2} at ~QIF. Pyroxene and plagioclase (An_{93-89}) saturation occurs early, and with continued crystallization, the residual liquid evolves to a silica-poor, halogen-, Fe-, and Ti-rich melt with a computed density of >3.1 g/cc. This liquid remains higher in density than the plagioclase over the crystallization interval, providing the possibility of plagioclase/melt separation by liquid draining.

A model is proposed in which "alkali" anorthosite, consisting of sodic anorthite or bytownite, coupled with underlying pyroxenite (or harzburgite) is produced locally during crystallization of plagioclase from "Al-rich" magmas at or within roughly a kilometer of the lunar surface. In this model, segregation of plagioclase would be attained by settling of ferromagnesian minerals to the bottom of a shallow magma chamber, and draining of low viscosity low silica, Fe-Ti-K-REE-P-enriched residual basaltic melt to deeper regions of the crust, or into topographic lows. Such residual melt may be represented by magma compositions similar to some of the intermediate to high Ti mare basalts. This model would provide a mechanism that can account for the more "alkali" anorthosite identified in widespread isolated locales on the Moon and allow for variable ages for such anorthosite that may extend to ages of the mare basalts.

Keywords: lunar Highlands, anorthosite, experimental petrology, fractional crystallization

Introduction

Ferroan anorthosite (FAN) has long been considered the dominant rock type of the primary lunar highlands crust. The lunar magma ocean (LMO) has been called upon as the means of generating the anorthositic crust of the highlands (e.g., Wood et al. 1970; Taylor and Jakes 1974). Current models of the LMO differ in depth and cooling rate (Warren 1985; Hess and Parmentier 1995; Elkins-Tanton, et al. 2002, 2012, and references therein); however, it is generally accepted that plagioclase flotation in the LMO eventually formed a cumulate lid at the surface of the Moon, and this primordial lunar crust is evidenced today as the FANs. In these models, all other lunar lithologies should post-date the anorthosites. Yet, recently collected geochronologic evidence suggests that FANs crystallized over an extended period of time, lasting more than 200 million years (Nyquist et al. 1995; Borg et al. 1999; 2011; Gaffney and Borg 2013). Lunar rock classes such as the Mg-suite and alkali suite, purportedly formed only

after almost complete solidification of the LMO and total crystallization of the FAN (James and Flohr 1983, Snyder et al. 1995). Compositions of classic FAN sampled from the lunar surface, and analyzed during the Apollo era consisted largely of anorthitic plagioclase (>An_{95}). The plagioclase grains in FAN are further characterized by almost invariant An contents in spite of a range in Mg number (e.g., Shearer and Papike 2005) of the host anorthosite. However, less calcic anorthosite that contains plagioclase more sodic than any found in the FAN samples has also been found (e.g., LG Y86032 anorthosite breccia clast, Nyquist et al. 2006; 116B Y86032 anorthosite breccia clast, Yamaguchi et al. 2010; 76504 F 18 anorthosite clast, Warren and Kallemeyn 1985; 14305,400 alkali anorthosite, Shervais et al. 1984; and a variety of other Apollo 14 alkali anorthosites analyzed by Warren in Lindstrom 1984).Taking for demonstration purposes two examples of these, plagioclase in Apollo sample 76504 has a typical An content of 91.3 +/- 0.7 (Warren and Kallemeyn 1985), with a range in composition from 89.9 to 93.3 (Warren et al. 1986). Although, Warren et al. (1986) describes it as an "evolved ferroan anorthosite," it does not have the highly anorthitic plagioclase of even the highly evolved hyperferroan anorthosites (Goodrich et al. 1984). Yamato-86032 is a breccia that contains multiple anorthosite fragments with plagioclase compositions ranging from 88.1 to 94.9 (Yamaguchi et al. 2010), placing them outside of the traditional FAN compositional range. Orbital data also show evidence for regions containing more albitic anorthosite than FAN. Ohtake et al. (2009) identified 69 individual regions on the lunar surface containing what they describe as pure anorthosite (areas containing >98% feldspar). These areas are limited in size, but have a broad range across the lunar surface. Greenhagen et al. (2010) collected Diviner spectral data, and measured the Christiansen Feature (CF) value of these terrains, which is useful for determining mineralogic composition of rocks at the surface. Of the analyzed areas, 15

contained what was termed as "intermediate composition" plagioclase, likely of labradorite/bytownite compositional range.

The nearly compositionally invariant character of plagioclase in FAN indicates that the less calcic plagioclase of alkali anorthosite with its Ab-enrichment with dropping temperature (as indicated by normal zoning) could not have directly evolved along the fractionation path that produced the characteristic plagioclase of FAN. Post-LMO magmatism in general appears to have been able to produce plagioclase less calcic than that of FAN with normal compositional evolution, as evidenced by plagioclase in the Mg- and alkali suite rocks and similar rock types as well as in mare basalts, with compositions ranging to An_{74} and lower (e.g., Shervais et al. 1984). These lithologies are not anorthosite, however, and the question arises whether plagioclase could float and accumulate in post-LMO magma bodies at or near the lunar surface to make them accessible for meteorite gardening and orbiter identification. This would require that the magma be saturated early with plagioclase at low pressure and that residual liquids become sufficiently dense to allow for crystal-melt separation by draining, leaving a plagioclase cumulate. Certainly impact melting of pre-existing FAN could produce secondary anorthosite, but this is unlikely to produce alkali anorthosite.

It is the goal of this study to experimentally assess whether lunar highlands basalt crystallizing at low pressure would produce the density conditions that would permit the formation of alkali anorthosite. Although this work uses a single "magma" composition, it is suggested that this process may have occurred in other post-LMO lunar magmas and that this process contributed to compositionally diversifying the lunar surface.

Sample Background

Only a limited number of non-mare rocks have been returned to Earth from the Moon that are both pristine and texturally suggest fast cooling and thus may be representative of a post LMO lunar highlands magma composition. Among these, the Apollo sample 14053 is particularly well studied. The specimen was found as a clast within a large brecciated boulder. It has a fine-grained texture typical of basalts, with crystals largely between 0.5 and 2 mm in length, although some pyroxenes exist up to 5 mm. Its bulk composition is similar to common terrestrial tholeiite (but with lower Na_2O content), and contains a mineral assemblage consistent with the experimental low-pressure phase assemblage (e.g., DiFrancesco et al.2013) as should be the case if it represents a liquid composition). Patchen and Taylor (2004) calculated modal abundances of minerals for this rock: 48% pyroxene, 42% plagioclase, 2.4% silica, 2.3% ilmenite, 1.6% olivine, >1% fayalite and Fe metal. Pyroxene and plagioclase show ophitic textures, with much of the plagioclase intergrown with the pyroxene, as noted by Kushiro et al. (1972). Plagioclase compositions from 14053,16 range from ~An_{80} (supplementary material) to An_{93} (Kushiro et al. 1972). Bence and Papike (1972) noted highly zoned pyroxene with compositions ranging from pigeonite to hedenbergite. A small amount of olivine is also present in the sample, with an analyzed composition of Fo_{66} (supplementary material). Kushiro (1972) also identified olivine grains present in the mesostasis, associated with cristobalite and metallic iron with a composition of $Fo_{13\text{-}14}$. Other crystalline phases include minor amounts of K-feldspar, apatite, ulvospinel, ilmenite and chromite. Patches of light brown glass also exist, which are associated with pyroxferroite. Reported glass compositions are potassic and rhyolitic (Kushiro et al. 1972).

Sample 14053 has been variously characterized as a low-Ti basalt (Papike et al. 1976), an aluminous mare basalt (Irving 1975), a mare-like basalt (Hubbard et al. 1972), and a pristine,

high Al basalt or diabase/microgabbro (Taylor et al. 2004; Hui et al. 2011; El Goresy et al. 1972). Chemically, it is distinct from mare basalts and KREEP basalts, having characteristically "high" Al, more similar to terrestrial basalt, yet the typical low alkalis of basaltic lunar lithologies (Hubbard et al. 1972). It shows a slight negative Eu anomaly (Hubbard et al. 1972) and is thus unlikely to have been formed after the removal of plagioclase or having attained its "high" Al characteristics by plagioclase accumulation. (Note: Further information on lunar basalt geochemistry can be found in Papike et al. 1998).

A well-recognized characteristic of sample 14053 is the occasional localized reduction of ferrous Fe in fayalite (Taylor et al. 2004; Patchen and Taylor 2004). However, the low fO_2 indicated by this reduction is likely not reflective of the magmatic source region; rather, it is considered to have occurred by hydrogenation from solar wind (Greenwood et al. 2010; Huss et al. 2012) during a heating event that occurred after crystallization, likely under subsolidus conditions (Taylor et al. 2004).As this process is unlikely to have affected the igneous mineralogy, it remains a good sample for this study of general post-LMO igneous processes.

Besides the major rock forming oxides, other constituents of a melt are important to consider, as they can affect the mineralogy and liquid evolution during crystallization. Evidence of volatiles in lunar magmas has been mounting; several workers have identified Cl and S in apatite grains from sample 14053 (e.g., Boyce et al. 2010) as well as in lunar basaltic glass inclusions (Saal et al. 2008), suggesting that volatiles can be retained after a magma has been erupted on the lunar surface. Secondary Ion Mass Spectrometry (SIMS) studies of apatite grains in 14053 indicate the presence of fluorapatite with significant OH content as well as F (McCubbin et al. 2010). While these apatite compositions are proof of dissolved volatiles in the melt during crystallization, the possibility of magmatic degassing (Nekvasil et al. 2010;

Ustunisik et al. 2011; Saal et al. 2008) and degassing during post-crystallization impact reheating makes any amounts present in residual glass highly unreliable. This uncertainty in magmatic volatile content made the choice of volatile abundances for the experiments a bit arbitrary; however, based on the discussions of McCubbin et al. (2011) and Boyce et al. (2010) we concluded that SO_2=0.2 wt%, Cl=0.5, F =0.5wt% would not be unreasonable. H_2O was omitted as an experimental component based on the results of Saal et al. (2008) and Ustunisik et al. (2011) who suggested rapid and effective degassing of OH at low pressure.

Experimental Design and Details

Experiments were designed to determine the compositional evolution of the residual melt and mineral phases of a magma having a composition approximately that of sample 14053 in equilibrium with metallic Fe undergoing equilibrium crystallization at low pressure. All experiments were crystallization experiments, in which the sample was melted above the liquidus temperature, cooled, and then allowed to equilibrate at a desired final temperature.

A synthetic mix approximating the bulk composition of 14053 (Table 1) was prepared using oxides, silicates, and Fe°sponge. The slight compositional differences between the synthetic mix and the published rock composition is not considered significant to this study of process rather than history of 14053. Cr was omitted from the synthetic mix to mitigate metastable chromite formation misrepresentative of natural processes. $MgCl_2$, MgF_2, and $CaSO_4$ provided the target values of 0.5 wt.% for Cl and F, and 0.3 wt.% for S. All major oxides were combined and ground with ethanol in an automatic mortar for two hours. MgF_2 and $MgCl_2$ were added towards the end of the mixing process in order to minimize dissolution and re-precipitation. Finally, Fe° was added with minimal ethanol in order to limit the amount of

159 settling and oxidation. The completed mix was ground for an additional 30 minutes, and dried in
160 air.

161 High purity Fe capsules measuring approximately 4mm (outer diamter) by 15mm long
162 were prepared with lids. Fe was chosen as a capsule material primarily to help constrain fO_2 near
163 the quartz-iron-fayalite buffer, as is typical of the lunar crust (Taylor et al. 2004). Capsules were
164 cleaned ultrasonically in acetone to remove any machining residue and reduced in H_2 at 800 °C.
165 For each experiment, a small amount of the powdered mix (~50 milligrams) was loaded into
166 each capsule and tamped down with a piston in order to pack the powder as densely as possible
167 and minimize pore space. Capsules were weighed and placed into a silica glass tube sealed at
168 one end. Just above the capsule, the open tube was then heated and stretched to form a small
169 capillary. A small chunk of Fe° as an "oxygen getter" was placed at the top of the capillary and
170 the tube was then evacuated for 15 minutes to remove as much air as possible. The entire
171 assembly was then lowered into a pot furnace, placing the sample near the hotspot at 800°C, and
172 the Fe° getter above it at ~600°C. The sample was dried for an additional 15 minutes to remove
173 any remaining moisture. The "getter" served to absorb any remaining oxygen in the tube to
174 prevent oxidation of the sample during heating. After the drying, a torch was used to sever and
175 seal the capillary just below the getter, preserving a vacuum in the silica glass ampoule. The
176 melted capillary was then formed into a hook for suspension.

177 A vertical tube, Pt-wound quench furnace was used for each experiment. The silica tube
178 was suspended by a thin Pt wire running through the hook at the top of the ampoule such that the
179 capsule was positioned at the experimentally determined hotspot of the furnace. A Pt_{90}-Rh_{10}
180 thermocouple, calibrated against the melting point of Au, was used to monitor the temperature of
181 the sample; it was positioned such that its tip was directly adjacent to the capsule. The capsule

and thermocouple were gradually lowered into the furnace in order to minimize thermal shock to the furnace. For each experiment, the sample was held at 1180°C for 1 hour after which the temperature was lowered to a crystallization temperature between 1140°C and 1015°C (that is, between the experimentally-determined liquidus and solidus temperatures for this system), cooling at approximately 15-20 degrees per minute (as necessitated by the furnace). The sample was kept at the crystallization temperature for between 2 and 150 hours. The duration of each experiment was dictated by attainment of homogeneous pyroxene compositions; the shortest-length experiments that produced homogenous (or near-homogenous) pyroxenes were used to maximize repeatability and minimize the chances for contamination or run failure. At the end of each experiment, a current was passed through the Pt wire supporting the sample, vaporizing it, and allowing the sample to fall into a beaker of cold water, thus, effectively quenching the capsule instantaneously (<5 sec) below the glass transition temperature. Temperatures above 1140°C yielded few (if any) crystalline phases, and temperatures below 1015°C were too crystalline to analyze easily and contained glass pockets that were no longer homogenous.

After quench, and before each silica glass tube was opened, it was checked to ensure a vacuum was maintained after quench. Then the Fe capsule was weighed to determine weight loss (if any), sawn open, and affixed to a glass slide to make a thin section. In some cases, shards of sample were removed from the capsule, placed in brass tubes, and encased in epoxy. These "slugs" were more conveniently analyzed by microprobe by allowing many samples in a single holder. We feel this allowed for more internally consistent analyses, since several samples could be analyzed in a single sample exchange/ standardization of the microprobe. Samples for microprobe analysis were carbon coated, and all phases resolvable by electron beam were analyzed using the Cameca SX100 electron microprobe at the American Museum of Natural

History, NY. An example backscatter electron image of an experiment taken during a microprobe session is available in the supplementary material. Most elements were analyzed using a 15kV accelerating voltage, 20nA beam current, a 5 micron beam diameter and measurement times of 20-40s per element. Na, K and F analyses were carried out using a defocused beam, a 2nA beam current, for 10-20s per element. Some phases were too small to analyze with a 5 um beam without overlapping onto glass. Fluorine analyses of glasses had the greatest (and unquantified) uncertainty due to the Fe-bearing nature of the glass. The following standards were used for most major element analyses: MgF_2, F; McKee Jadeite, Na; Potassium Feldspar, K; San Carlos Olivine, Mg; Wakefield Plagioclase, Si and Ca; Berlinite, P; Barite, S; Scapolite, Cl; Rutile, Ti; $MgCr_2O_4$, Cr; Rhodonite, Mn; Fayalite, Fe. Mass balance calculations (MIX program of the IgPet software package, Carr 2002) were conducted using the microprobe data in order to ascertain that no phases had been overlooked, to ensure internal consistency of phase compositions, and to obtain modal abundances of phases.

Results

All experiments yielded either glass or glass + crystals. Figure 1 shows the mode of each experiment computed by mass balance; Table 2 shows the average composition for each analyzed phase. Ilmenite, silica, and Fe° minerals were observed in EDS, but were too small to be easily analyzed by the microprobe. Therefore, ideal stoichiometric compositions of these were used in place of actual analyses for mass balance. The lowest temperature experiment (1015°C) was so fine-grained that many analyses reflected overlap of small mineral grains; therefore, for the purposes of the least squares regression, the average liquid analyzed from that experiment was used together with plagioclase and pyroxene compositions taken from the next highest temperature (1055°C).

The dominant phases in both sets of experiments were pyroxene and plagioclase – in agreement with the mineralogic mode of 14053. Although olivine crystallized early in the experiments, it reacted out as pyroxene began to form. It was noted that pyroxene compositions were highly variable in experiments that had not attained equilibrium (unpublished data); therefore, pyroxene was used as a proxy for measuring the degree of disequilibrium in each experiment. For this purpose we used the QUILF 95 software (Andersen et al. 1993) to project pyroxene and olivine compositions. Runs that did not attain equilibrium (i.e., had highly variable pyroxene compositions) were rejected and the experiments repeated for a longer duration. Pyroxenes in our experiments generally increased in Fs and Wo components with decreasing temperature (Fig. 2).

Plagioclase begins to crystallize at 1100°C, a lower temperature than pyroxene, yet while there is still more than 60% liquid remaining. Plagioclase compositions were computed based on the molar quantities of Ca, Na, and K (Fig. 3). Slight modification of silica and alumina contents within microprobe uncertainty was required to obtain stoichiometric compositions. Plagioclase composition varied from An_{93} to An_{89}, but it was difficult to evaluate the trend with decreasing temperature since the relatively slow cooling to the equilibration temperature may have caused earlier formed plagioclase to be retained as suggested by the range and overlap of the plagioclase compositions for the temperatures at which plagioclase was stable. The observation that the lower temperature (1055^{o}C) experiment had more anorthitic plagioclase than the 1100^{o}C experiment we attribute to the fine-grained nature of the lower temperature experiment, and the resulting difficulty in analyzing the last formed plagioclase, that is, the lowest temperature plagioclase composition of the outermost zone of the zoned crystals. Importantly, the feldspars show that the earliest formed plagioclase is more albitic than the FAN (even within the 2% probe

error), and the plagioclase is produced with compositions that extend to bytownite. Finally, due to known Na-loss issues during analysis with EMPA, it is possible that the actual Ab contents of the plagioclase are slightly higher than the averaged reported values. Therefore, since the compositional range of the plagioclase analyzed here does not overlap the FAN field, we are confident that this process can produce plagioclase of a composition unique from that of the ferroan anorthosites, and similar to that of the alkali anorthosite suite.

Figure 4 shows the change in major oxide concentrations of experimental residual liquids (glasses) with decreasing temperature. The silica content does not increase, even after 80% crystallization, but rather remains almost constant before decreasing in late stages. The alumina content of the melt shows the expected variation that is, increasing until plagioclase saturation and then decreasing due to plagioclase precipitation. FeO_T initially shows a slight decrease, but generally increases in the melt. Titania increases in concentration until ilmenite appears, at which point TiO_2 is drawn out of the melt. Importantly, there is strong enrichment of F and Cl in the liquid with decreasing temperature (Fig. 5), rather than the losses observed by Ustunisik et al. (2011).

Discussion

Pyroxene and plagioclase are the dominant minerals in the crystallizing assemblage. The plagioclase is not the extremely calcic plagioclase of FAN, but rather ranges from more sodic anorthite to bytownite in composition, typical of Mg-suite norites which have plagioclase compositions ranging from An_{93} to An_{88} (James and Flohr 1983). Of particular importance is the increase in Fe and Ti of the residual liquids, which also correlates to an increase in Cl content of the residual melts with decreasing temperature. These results are consistent with the work of Webster and DeVivo (2002) that showed an increased solubility of Cl in low silica, Fe-rich

melts, perhaps due to Fe-Cl complexing in the melt; such complexing may have contributed to the strong Fe-enrichment of the melt during crystallization. It is possible that halogens also facilitate Ti buildup in the melt through the formation of TiF_4 and $TiCl_4$ complexes, both of which would allow Ti to build up in the melt beyond the point where armalcolite or ilmenite (+rutile) would normally be stable.

The buildup of Cl and F in the melt appears contradictory to the results of Ustunisik et al. (2011) who detected continuous loss of F and Cl during degassing under similar experimental conditions. However, this loss may have been facilitated by the presence of H_2O in their experiments and hence, loss of HCl and HF, in addition to the lack of mineralogically-driven Fe enrichment of the melt that would retain Cl, since their experiments were superliquidus. Another major driver of this increase in F and Cl is the absence of apatite in the mineral assemblage; however, there is no indication that this is an experimental problem. The highest residual liquid P_2O_5 concentration attained is 0.42 wt.% (Table 2); this is below the concentration necessary to stabilize apatite in a magma with this silica content (Watson 1979). Also, the CIPW norm calculation (supplementary material) for this liquid composition contains less than 1 wt.% apatite; thus, its absence cannot account for more than a fraction of this increase in halogens in the residual melt. These results suggest that lunar magmas would be able to retain substantial amounts of volatiles, even near the surface before completely crystallizing.

An important result of the Fe- and Ti-enrichment of residual liquids is a general increase in density of the liquid. Figure 6 shows liquid densities computed using the techniques of Lange and Carmichael (1987) assuming that both F and Cl in the melt have the partial molar volume of water (with the goal of computing a minimum density) at each temperature. The concentration of these elements in the melt, coupled with the "stagnation" of the silica content helps to keep the

297 liquid density high, reaching a peak of 3.23 g/cc at 1055°C. This contrasts with the lower
298 densities of anorthite (2.76 g/cc) and pigeonite (3.38 g/cc) (Klein et al. 2002). Importantly, there
299 is no spike in density; rather, the density remains relatively uniform, allowing a significant
300 period of crystallization over which plagioclase and pyroxene could separate through density
301 stratification.

302 In the case of a magma chamber close to the lunar surface, plagioclase flotation is
303 probably not a relevant process. Instead, liquid draining is a more likely method to induce
304 plagioclase separation, particularly in the anorthositic highlands crust. Liquid draining has been
305 postulated in terrestrial layered intrusions such as the Bushveld complex in South Africa (Scoon
306 and Mitchell 1994). Importantly, with a lower layer of pyroxene cumulates more dense than the
307 liquid, the residual liquid would not necessarily have drained to deeper levels of the crust, but
308 perhaps flowed laterally into topographic lows (much as groundwater flows laterally, pressurized
309 by a hydraulic head) and solidified at the lunar surface, forming sheets of Fe- and Ti-basaltic
310 rock that would show K, REE, and P enrichment and a strong negative Eu anomaly. Loss of this
311 liquid would leave behind bimodal lithologies of overlying anorthosite and underlying
312 pyroxenite (or dunite if from a less evolved starting magma than 14053). Since such a process is
313 not restricted in time, could the mobilized liquid be represented by some mare basalts?

314 It has been suggested that the source material for the aluminous basalts, including 14053,
315 is very similar to the areas of the mantle which have given rise to the mare basalts (Ridley 1975);
316 indicating the recognition of geochemical similarities. The high Ti, and Fe nature of some of the
317 Apollo 12 mare (ilmenite) basalts is strikingly similar to the residual liquids produced during
318 crystallization of 14053. For example, Apollo samples 12054, and 12047, mare basalts collected
319 from the Ocean of Storms during Apollo 12 are nearly identical (within analytical error) in

composition to the residual liquid at 1055°C (Rhodes et al. 1977). Apollo 15 sample 15388 is chemically similar to these same liquids as well, although there is a large discrepancy in Mg content (Ryder et al. 1988). (These samples are presented to facilitate comparison in Table 3.) Interestingly, both Apollo 12 samples appear to contain slight negative Eu anomalies characteristic of magmas that have seen plagioclase removal, which is permissive of residual liquids leftover from anorthosite formation. It should be stressed again that we are not supposing that Apollo basalt 14053 is parental to any of these specific samples, rather that crystal fractionation of a typical lunar high-Al basalt at low pressure is able to produce a variety of rock compositions observed at the lunar surface. Nyquist and Shih (1992) provide evidence demonstrating that aluminous basalts were being produced over a long period of time on the Moon (4.3-3.1 Ga), a period that brackets the age of many Ti-basalts (3.9-3.5 Ga) and alkali anorthosites (4.3-4.0 Ga, Snyder et al. 1995). If this aluminous basalt volcanism was not limited to Fra Mauro, it is possible that the magmas could have experienced conditions similar to what we have modeled here, and produced pockets of sodic anorthosites and/or basalts with compositions comparable to the ilmenite basalts of Apollo 12 and 15. We must concede however, that there is no direct observational evidence supporting this, but because of current remote-sensing limitations and the extremely brecciated nature of the lunar crust, it would be very difficult to observe spatial relationships between these rock suites in situ.

Implications

The experiments conducted show the potential for Cl- and F-bearing aluminous basalts from the lunar highlands to produce anorthosite independent of the LMO, thereby providing a mechanism that could explain the existence of isolated areas of alkali anorthosite, allow such anorthosite to be less calcic than FAN, and explain variable absolute ages as well as relative ages

with respect to other lunar lithologies. The observed buildup of halogens in the melt and concomitant Fe- and Ti- enrichment makes it possible for the residual liquid to drain from the overlying plagioclase and pond as a silica-poor Fe-and Ti-rich basalt with K-REE-P enrichment and negative Eu anomaly. However, it is important to note the role of F and Cl in this process is not fully understood.

Acknowledgements

Our EMPA were carried out at the American Museum of Natural History's Electron Microprobe Facility with the generous assistance of J. Gross. We are grateful to A. Coraor for his help throughout the experimental and analytical process. We appreciate the helpful comments of R. Tartèse, and an anonymous reviewer which served to improve the manuscript. Finally, the authors thank the Associate Editor, P. Isaacson for his editorial handling. This work was supported by NASA grant NNX08AZ04G to HN.

References

Andersen, D.J., Lindsley, D.H., and Davidson, P.M. (1993) QUILF: A pascal program to assess equilibria among Fe- Mg- Mn- Ti- oxides, pyroxenes, olivine, and quartz. Computers and Geosciences, 19(9), 1333-1350.

Bence, A., and Papike, J. (1972) Pyroxenes as recorders of lunar basalt petrogenesis: Chemical trends due to crystal-liquid interaction. Lunar and Planetary Science Conference Proceedings, 3, 431.

Borg, L., Norman, M., Nyquist, L., Bogard, D., Snyder, G., Taylor, L., and Lindstrom, M. (1999) Isotopic studies of ferroan anorthosite 62236: a young lunar crustal rock from a light rare-earth-element-depleted source. Geochimica et Cosmochimica Acta, 63(17), 2679-2691.

Borg, L.E., Connelly, J.N., Boyet, M., and Carlson, R.W. (2011) Chronological evidence that the Moon is either young or did not have a global magma ocean. Nature, 477(7362), 70-72.

Boyce, J.W., Liu, Y., Rossman, G.R., Guan, Y., Eiler, J.M., Stolper, E.M., and Taylor, L.A. (2010) Lunar apatite with terrestrial volatile abundances. Nature, 466(7305), 466-469.

Carr, M. (2002) IGPET for Windows. Terra Softa, Somerset, NJ.

DiFrancesco, N. J., Nekvasil, H., Ustunisik, G., & Lindsley, D. H. (2013, March). Evolved Melts from Lunar Highlands Basalts: Can they Produce Lunar Granites?. In Lunar and Planetary Institute Science Conference Abstracts (Vol. 44, p. 2619).

El Goresy, A., Taylor, L.A., and Ramdohr, P. (1972) Fra Mauro crystalline rocks: Mineralogy, geochemistry, and subsolidus reduction of the opaque minerals. Lunar and Planetary Science Conference Proceedings, 3, 333.

Elkins-Tanton, L. T., Van Orman, J. A., Hager, B. H., & Grove, T. L. (2002). Re-examination of the lunar magma ocean cumulate overturn hypothesis: melting or mixing is required. Earth and Planetary Science Letters, 196(3), 239-249.

Elkins-Tanton, L.T., Burgess, S., and Yin, Q-Z. (2011) The lunar magma ocean: Reconciling the solidification process with lunar petrology and geochronology. Earth and Planetary Science Letters, 304(3), 326-336.

Gaffney, A.M., and Borg, L.E. (2013) A young age for KREEP formation determined from Lu-Hf isotope systematics of KREEP basalts and Mg-Suite Samples. Lunar and Planetary Science Conference XLIV, CD-ROM no. 1714. Lunar and Planetary Institute, Houston.

Goodrich, C. A., Taylor, G. J., Keil, K., Boynton, W. V., & Hill, D. H. (1984). Petrology and chemistry of hyperferroan anorthosites and other clasts from lunar meteorite ALHA81005. Journal of Geophysical Research: Solid Earth, 89(S01), C87-C94.

Greenhagen, B.T., Lucey, P.G., Wyatt, M.B., Glotch, T.D., Allen, C.C., Arnold, J.A., Bandfield, J.L., Bowles, N.E., Hanna, K.L.D., Hayne, P.O., Song, E., Thomas, I.R., and Paige, D.A. (2010) Global silicate mineralogy of the Moon from the Diviner Lunar Radiometer. Science, 329(5998), 1507-1509.

Greenwood, J., Itoh, S., Sakamoto, N., Taylor, L., Warren, P., and Yurimoto, H. (2010) Water in Apollo rock samples and the D/H of lunar apatite. Lunar and Planetary Institute Science Conference, XLI, CD-ROM no. 2439. Lunar and Planetary Institute, Houston.

Hess, P.C., Parmentier, E.M. (1995). A model for the thermal and chemical evolution of the moon's interior: implications for the onset of mare volcanism. Earth and Planetary Science Letters, 134, 501–514.

Hubbard, N., Gast, P., Rhodes, J., Bansal, B., Wiesmann, H., and Church, S. (1972) Nonmare basalts: part II. Lunar and Planetary Science Conference Proceedings, 3, 1161.

Hui, H., Oshrin, J.G., and Neal, C.R. (2011) Investigation into the petrogenesis of Apollo 14 high-Al basaltic melts through crystal stratigraphy of plagioclase. Geochimica et Cosmochimica Acta, 75(21), 6439-6460.

Huss, G., Nagashima, K., Burnett, D., Jurewicz, A., and Olinger, C. (2012) A new upper limit on the D/H ratio in the solar wind. Lunar and Planetary Institute Science Conference XLIII, CD-ROM no. 1709. Lunar and Planetary Institute, Houston.

Irving, A.J. (1975) Chemical, mineralogical and textural systematics of non-mare melt rocks Implications for lunar impact and volcanic processes. Lunar and Planetary Science Conference Proceedings, 6, 363-394.

James, O.B. and Flohr, M.K. (1983) Subdivision of the Mg-suite noritic rocks into Mg-gabbronorites and Mg-norites. Journal of Geophysical Research, 88, S02, p. A603-A614.

Klein, C., Hurlbut, C. S., & Dana, J. D. (2002). The 22nd edition of the manual of mineral science:(after James D. Dana).

Kushiro, I., Ikeda, Y., and Nakamura, Y. (1972) Petrology of Apollo 14 high-alumina basalt. Lunar and Planetary Science Conference Proceedings, 3, 115.

Lange, R.A., and Carmichael, I.S. (1987) Densities of Na_2O-K_2O-MgO-MgO-FeO-Fe_2O_3-Al_3O3-TiO_2-SiO_2 liquids: New measurements and derived partial molar properties. Geochimica et Cosmochimica Acta, 51, 2931-2946.

Lindstrom, M. M. (1984). Alkali gabbronorite, ultra-KREEPy melt rock and the diverse suite of clasts in North Ray Crater feldspathic fragmental breccia 67975. Journal of Geophysical Research: Solid Earth, 89(S01), C50-C62.

McCubbin, F.M., Steele, A., Hauri, E.H., Nekvasil, H., Yamashita, S., and Hemley, R.J. (2010) Nominally hydrous magmatism on the Moon. Proceedings of the National Academy of Sciences, 107(25), 11223-11228.

McCubbin, F. M., Jolliff, B. L., Nekvasil, H., Carpenter, P.K., Zeigler, R.A., Steele, A, Elardo, S.M., and Lindsley, D. H. (2011). Fluorine and chlorine abundances in lunar apatite: Implications for heterogeneous distributions of magmatic volatiles in the lunar interior. Geochimica et Cosmochimica Acta, 75(17), 5073-5093.

Nekvasil, H., McCubbin, F., and Ustunisik, G. (2010) Using apatite to assess volatile contents of primary lunar magmas: Potential pitfalls. AGU Fall Meeting Abstracts, 1, p. 05.

Nyquist, L. and Shih, C.-Y. (1992). The isotopic record of lunar volcanism. Geochimica et Cosmochimica Acta, 56(6), 2213-2234.

Nyquist, L., Wiesmann, H., Bansal, B., Shih, C.-Y., Keith, J., and Harper, C. (1995) ^{146}Sm-^{142}Nd formation interval for the lunar mantle. Geochimica et Cosmochimica Acta, 59(13), 2817-2837.

Nyquist, L., Bogard, D., Yamaguchi, A., Shih, C. Y., Karouji, Y., Ebihara, M., ... & Takeda, H. (2006). Feldspathic clasts in Yamato-86032: Remnants of the lunar crust with implications for its formation and impact history. Geochimica et cosmochimica acta, 70(24), 5990-6015.

Ohtake, M. et al. (2009). The global distribution of pure anorthosite on the Moon. Nature, 461 236-240.

Papike, J., Hodges, F., Bence, A., Cameron, M., and Rhodes, J. (1976) Mare basalts: Crystal chemistry, mineralogy, and petrology. Reviews of Geophysics, 14(4), 475-540.

Papike, James Joseph, G. Ryder, and C. K. Shearer. Planetary materials. Chantilly, VA: Mineralogical Society of America, 1998.

Patchen, A., and Taylor, L. (2004) The most reduced rock from the Moon—Apollo 14 basalt 14053: Extreme reduction entirely from a re-heating event. Lunar and Planetary Science Conference XXXV, CD-ROM no. 1762. Lunar and Planetary Institute, Houston.

Rhodes, J.M., Brannon, J.C., Rodgers, K.V., Blanchard, D.P. and Dungan, M.A. (1977). Chemistry of Apollo 12 mare basalts-Magma types and fractionation processes. Lunar and Planetary Science Conference Proceedings, 8, 1305-1338.

Ridley, W.I. (1975) On high-alumina mare basalts. Lunar and Planetary Science Conference Proceedings, 6, 131-145.

Ryder, G. and Steele, A. (1988). Chemical dispersion among Apollo 15 olivine-normative mare basalts. Lunar and Planetary Science Conference Proceedings, 18, 273-282.

Saal, A.E., Hauri, E.H., Cascio, M.L., Van Orman, J.A., Rutherford, M.C., and Cooper, R.F. (2008) Volatile content of lunar volcanic glasses and the presence of water in the Moon's interior. Nature, 454(7201), 192-195.

Scoon, R.N., and Mitchell, A.A. (1994) Discordant iron-rich ultramafic pegmatites in the Bushveld Complex and their relationship to iron-rich intercumulus and residual liquids. Journal of Petrology, 35(4), 881-917.

Shearer, C. K., & Papike, J. J. (2005). Early crustal building processes on the moon: Models for the petrogenesis of the magnesian suite. Geochimica et Cosmochimica Acta, 69(13), 3445-3461.

Shervais, J.W., Taylor, L.A., Laul, J.C., and Smith, M.R. (1984) Pristine highland clasts in Consortium Breccia 14305: Petrology and geochemistry. Journal of Geophysical Research: Solid Earth, 89(S01), C25-C40.

Snyder, G.A., Taylor, L.A., Halliday, A.N. (1995) Chronology and petrogenesis of the lunar highlands alkali suite: Cumulates from KREEP basalt crystallization. Geochimica et Cosmochimica Acta, 59(6), 1185-1203.

Taylor, L.A., Patchen, A., Mayne, R.G., and Taylor, D.-H. (2004) The most reduced rock from the moon, Apollo 14 basalt 14053: Its unique features and their origin. American Mineralogist, 89(11-12), 1617-1624.

Taylor, S., and Jakes, P. (1974) The geochemical evolution of the Moon. Lunar and Planetary Science Conference Proceedings, 5, 1287-1305.

Ustunisik, G., Nekvasil, H., and Lindsley, D. (2011) Differential degassing of H_2O, Cl, F, and S: Potential effects on lunar apatite. American Mineralogist, 96(10), 1650-1653.

Warren, P. H. (1985). The magma ocean concept and lunar evolution. Annual Review of Earth and Planetary Sciences, 13(1), 201-240.

Warren, P.H., and Kallemeyn, G.W. (1985) "New" pristine moon rocks: augite-rich Ferroan Anorthosite 76504,18-the link between ferroan anorthosites and mare basalt source regions? Lunar and Planetary Science Conference XVI. 893-894. Lunar and Planetary Institute, Houston.

Warren, P. H. (1986). Anorthosite assimilation and the origin of the Mg/Fe-related bimodality of pristine moon rocks: Support for the magmasphere hypothesis. Journal of Geophysical Research: Solid Earth, 91(B4), 331-343.Watson, B.E. (1979) Apatite saturation in basic to intermediate magmas. Geophysical Research Letters, 6 (12), 937-940.

Watson, E. B. (1979). Apatite saturation in basic to intermediate magmas. Geophysical Research Letters, 6(12), 937-940.

Webster, J.D., and De Vivo, B. (2002) Experimental and modeled solubilities of chlorine in aluminosilicate melts, consequences of magma evolution, and implications for exsolution of hydrous chloride melt at Mt. Somma-Vesuvius. American Mineralogist, 87(8-9), 1046-1061.

Willis, J.P., Erlank, A.J., Gurney, J.J., Theil, R.H., and Ahrens, L.H. (1972). Major, minor, and trace element data for some Apollo 11, 12, 14 and 15 samples. Lunar and Planetary Science Conference Proceedings, 3, 1269-1273.

Wood, J.A., Dickey Jr, J., Marvin, U.B., and Powell, B. (1970) Lunar anorthosites and a geophysical model of the moon. Geochimica et Cosmochimica Acta Supplement, 1, 965.

Yamaguchi, A., Karouji, Y., Takeda, H., Nyquist, L., Bogard, D., Ebihara, M., Shih, C.Y., Reese, Y., Garrison, D., Park, J., and McKay, G. (2010) The variety of lithologies in the Yamato-86032 lunar meteorite: Implications for formation processes of the lunar crust. Geochimica et Cosmochimica Acta, 74(15), 4507-4530.

Table Captions

Table 1: Comparison of bulk rock analysis of Apollo sample 14053 (Willis et al. 1972) to the composition of the prepared synthetic starting material (VOL).

512 Table 2: Electron microprobe analysis showing average compositions of phases (minerals and
513 glass) from each experiment. Abbreviations used: pyroxene (Px); plagioclase (Pl); olivine (Ol);
514 glass/liquid (Gl). Numbers in parenthesis indicate the number of averaged points. "Other
515 Phases" include a natural ilmenite analysis (Ilm), as well as nominal compositions for iron metal
516 and amorphous silica. The abundance (wt. %) of each phase (and sums of the squares of the
517 residuals, *ssr*) were calculated by mass balance (Carr 2002). Molar An# = An/(An+Ab), molar
518 Mg# = MgO/(MgO+FeO).

519 Table 3: Comparison of residual liquid composition from 1055^{o}C with compositions of ilmenite
520 basalts recovered from Apollo 12 (Rhodes et al. 1977) and Apollo 15 (Ryder et al. 1988).

521 Table S1: Electron microprobe analysis of phases present in Apollo sample 14053.

522

523 Figure Captions

524 Figure 1: Phase-abundance diagram illustrating the amount of crystals and liquid for each
525 experiment as computed by mass balance (Carr 2002).

526 Figure 2: A pyroxene quadrilateral showing the compositions of experimental pyroxenes from
527 experiments at various temperatures. The grouping of pyroxenes at 1140^{o}C is connected by tie-
528 line to the coexisting olivine at that temperature. Arrow illustrates compositional trend with
529 decreasing temperature.

530 Figure 3: A truncated feldspar ternary diagram showing analyzed plagioclase compositions
531 (high and low An) for experiments at each temperature. Ellipses around markers delineate the
532 range of plagioclase compositions for each experiment- solid ellipse - 1100^{o}C, dashed ellipse-

533 1055^{o}C. Markers are sized to estimate the analytical uncertainty. Approximate boundaries are
534 drawn to show the extent of the FAN (upper shaded ellipse) and Mg- suites (large ellipse).

535 Figure 4: Concentrations (weight percent) of select oxides in residual liquids for each
536 experiment. Error bars for silica represent a 2% absolute variation. All other uncertainties are
537 approximately similar in size to, or smaller than markers used.

538 Figure 5: Concentrations of volatiles in residual liquids determined for each experiment.

539 Figure 6: Calculated density (Lange and Carmichael 1987) of residual liquids from each
540 experiment. Density of pyroxene (pigeonite) and plagioclase (anorthite) are also shown (Klein et
541 al. 2002).

542 Figure S1: Backscattered electron image of an experiment at 1100^{o}C showing all phases present-
543 pyroxene, plagioclase and glass, as well as the Fe capsule wall.

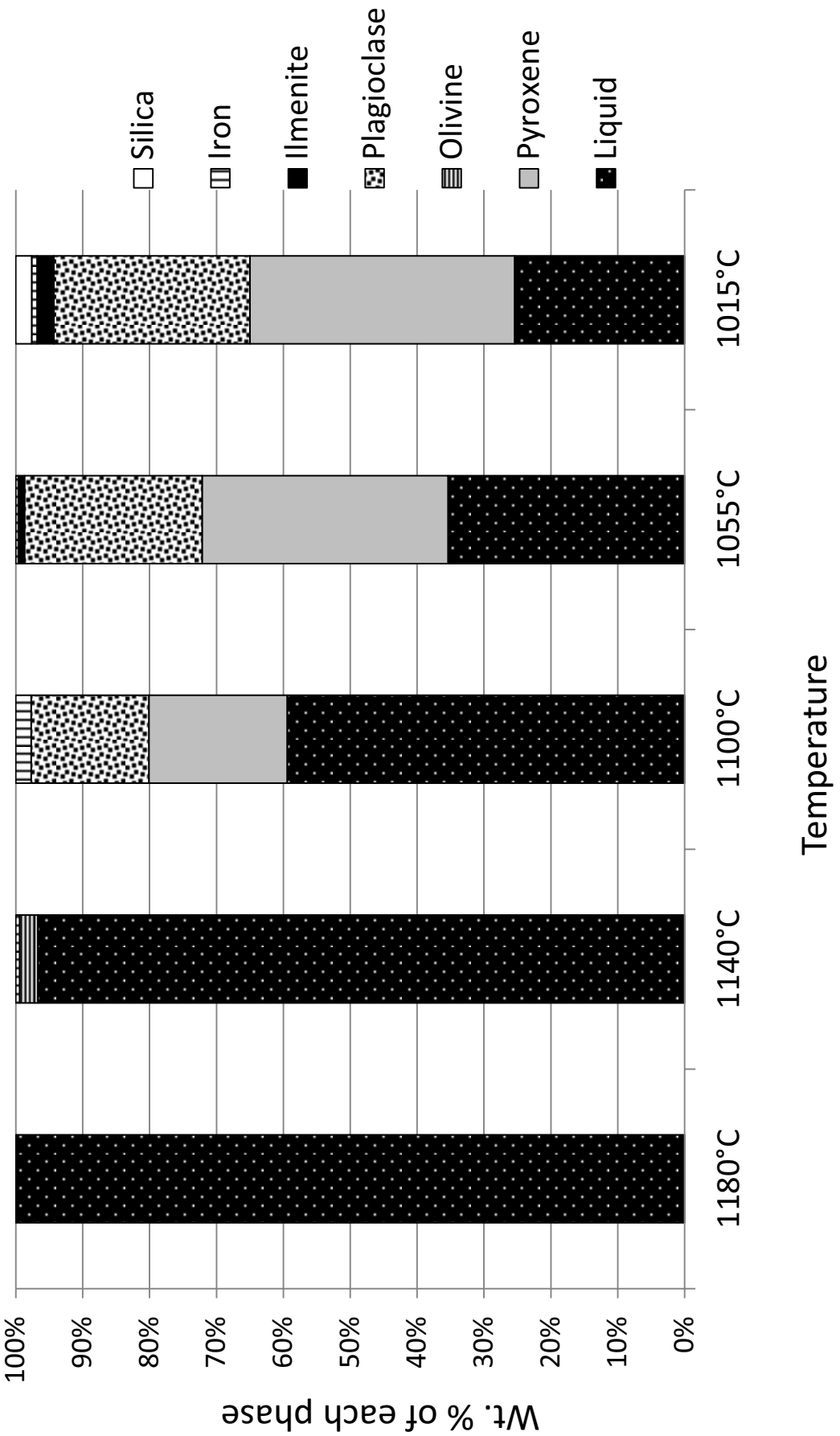
Silica
Iron
Ilmenite
Plagioclase
Olivine
Pyroxene
Liquid
1015°C
1055°C
1100°C
1140°C
1180°C
Temperature
100%
90%
80%
70%
60%
50%
40%
30%
20%
10%
0%
Wt. % of each phase

Figure 1

Figure 2

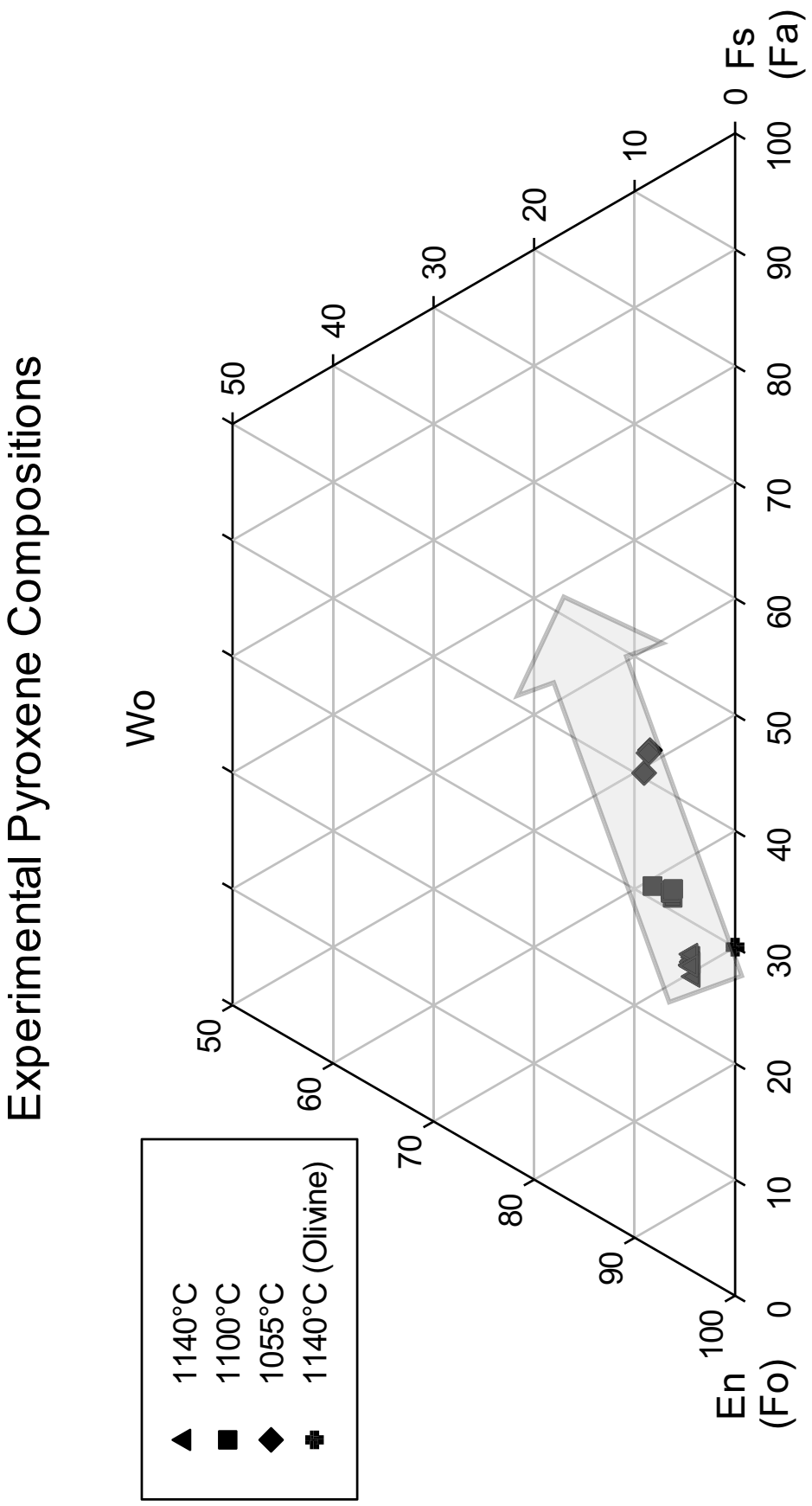
Experimental Pyroxene Compositions
Wo
50
40
30
20
10
0 Fs (Fa)
50
60
70
80
90
100 En (Fo)
0
10
20
30
40
50
60
70
80
90
100
1140°C
1100°C
1055°C
1140°C (Olivine)

Figure 3

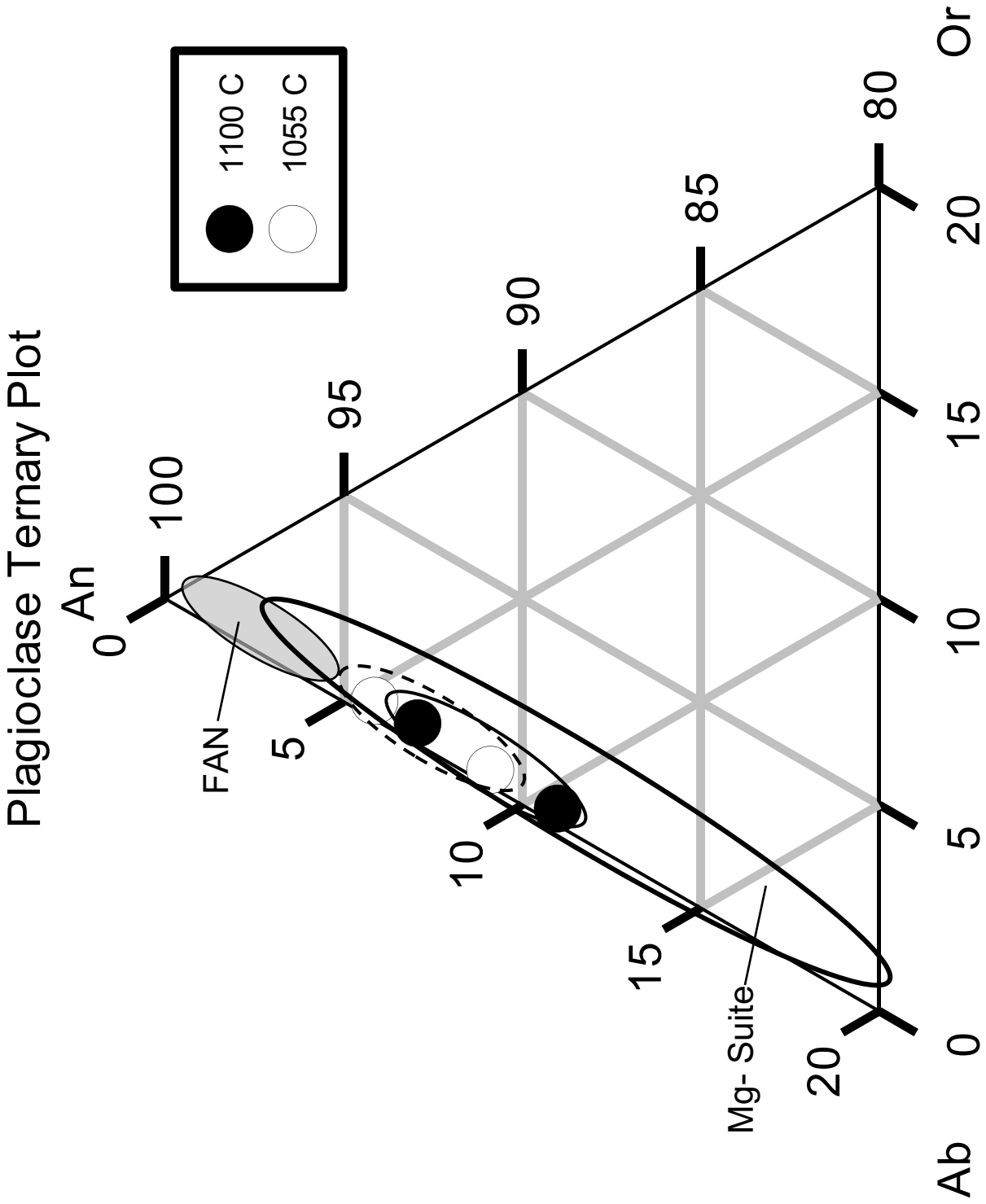
Plagioclase Ternary Plot
An
Ab
Or
0
100
95
90
85
80
5
10
15
20
0
5
10
15
20
1100 C
1055 C
FAN
Mg- Suite

	14053	VOL
SiO_2	46.08	45.94
TiO_2	2.91	2.83
Al_2O_3	12.54	12.66
FeO	16.97	17.83
MnO	0.26	0.23
MgO	8.97	7.66
CaO	11.07	10.21
Na_2O	0.44	0.49
K_2O	0.1	0.13
P_2O_5	0.11	0.07
Cr_2O_5	0.28	-
SO_2	0.13	0.21
Cl	-	0.45
F	-	0.51

Table 1

Temperature	1140 C					1100 C						1055 C						1015 C		Other Phases		
Phases	Px (11)	1σ	Ol (1)	Gl (13)	1σ	Px (6)	1σ	Pl (9)	1σ	Gl (10)	1σ	Px (3)	1σ	Pl (4)	1σ	Gl (18)	1σ	Gl (3)	1σ	Ilm	Iron	Silica
SiO2	52.43	0.55	37.02	46.22	1.08	51.76	0.66	47.11	0.46	45.92	0.72	48.57	1.82	45.99	0.30	45.39	0.32	43.27	1.17	0.11	0	100
TiO2	0.68	0.07	0.05	2.91	0.09	0.98	0.10	0.08	0.03	4.32	0.07	1.22	0.18	0.19	0.15	5.30	0.09	4.04	0.10	48.9	0	0
Al2O3	1.95	0.09	0.01	13.30	0.33	2.11	0.25	33.33	0.44	10.85	0.14	1.84	0.18	33.23	1.16	9.34	0.22	8.99	0.45	0.54	0	0
FeO	17.17	0.16	27.78	17.20	0.21	19.82	0.31	0.58	0.05	19.26	0.41	25.60	0.84	1.42	0.56	20.48	0.25	20.36	0.53	48	100	0
MnO	0.32	0.03	0.24	0.25	0.02	0.44	0.02	0.01	0.02	0.35	0.02	0.39	0.02	0.02	0.02	0.26	0.03	0.30	0.02	0	0	0
MgO	25.18	0.08	35.98	7.14	0.75	21.81	0.26	0.32	0.04	5.30	0.05	16.97	0.28	0.29	0.09	3.92	0.07	3.41	0.02	0.35	0	0
CaO	2.19	0.10	0.22	10.67	0.09	3.24	0.39	17.64	0.30	10.86	0.08	4.15	0.13	18.00	0.29	11.28	0.13	12.86	0.10	0.56	0	0
Na2O	0.05	0.08	0.04	0.40	0.07	0.02	0.04	0.97	0.14	0.38	0.04	0.04	0.06	0.81	0.18	0.43	0.07	0.59	0.06	0.65	0	0
K2O	0.02	0.04	0.02	0.11	0.02	0.01	0.01	0.04	0.03	0.15	0.03	0.02	0.02	0.07	0.02	0.21	0.04	0.32	0.05	0	0	0
P2O5	0.01	0.01	0.05	0.10	0.01	0.01	0.01	0.01	0.01	0.11	0.02	0.01	0.01	0.01	0.01	0.24	0.02	0.42	0.02	0	0	0
SO2	0.01	0.01	0.00	0.11	0.01	0.01	0.01	0.00	0.01	0.21	0.01	0.01	0.00	0.03	0.03	0.25	0.09	0.21	0.10	0	0	0
Cl	0.01	0.01	0.00	0.47	0.01	0.00	0.00	0.00	0.00	0.70	0.01	0.01	0.01	0.03	0.03	0.94	0.01	2.23	0.07	0	0	0
F	0.07	0.14	0.12	0.48	0.18	0.00	0.00	0.02	0.04	0.54	0.08	0.22	0.33	0.06	0.08	1.04	0.23	1.97	0.42	0	0	0
Total	100.06		101.52	99.35		100.19		100.12		98.94		99.04		100.13		99.09		98.97		99.1	100	100
Wt. % Phase	0.5		2.2	96.7		20.7		17.6		59.4		36.8		26.6		35.4		25.4				
Residual Sum	0.055					0.018						0.016						0.009				
An# or Mg#	72		70(XFo)	-		62		91			-	52		93			-		-			

Figure 4

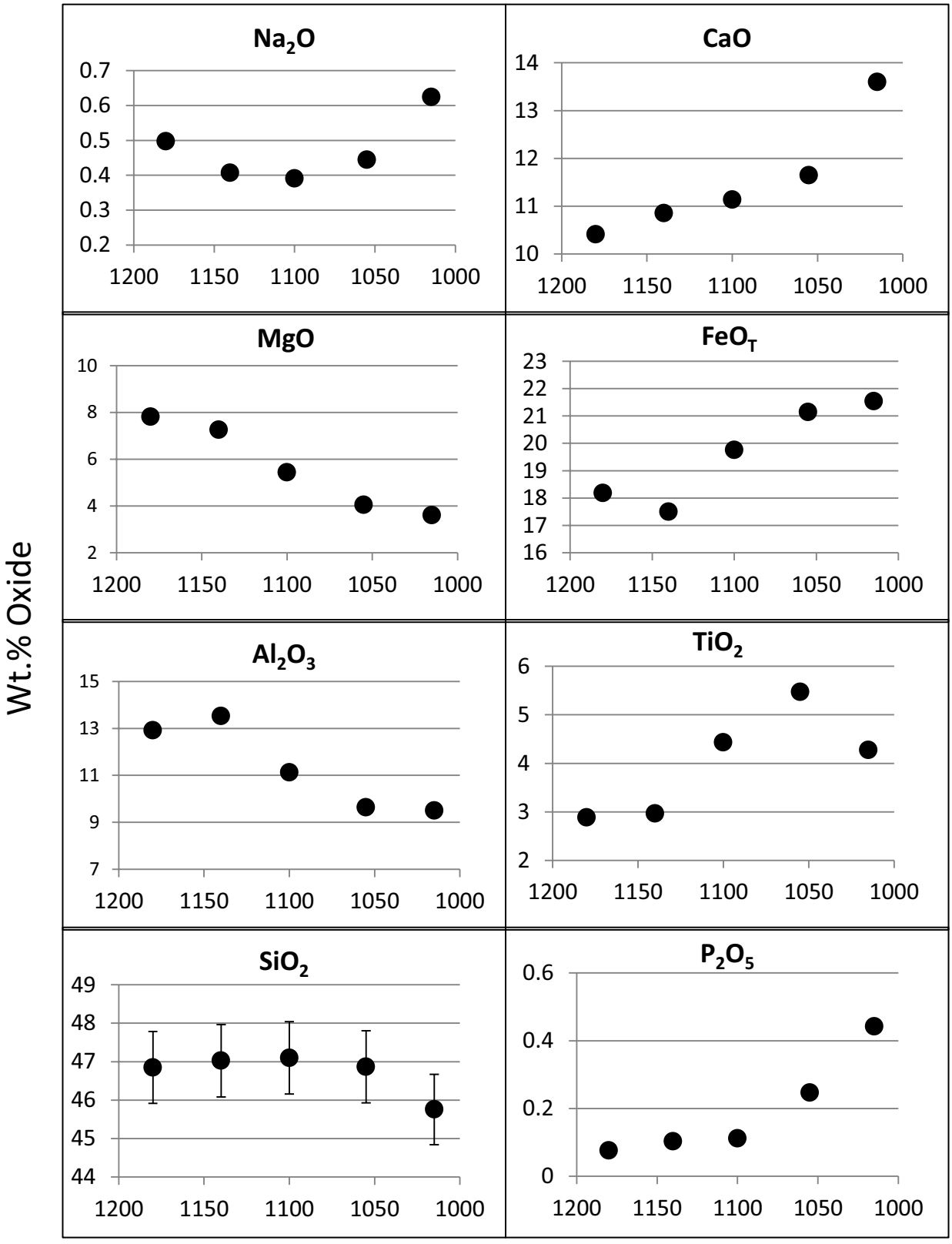
Na2O
0.7
0.6
0.5
0.4
0.3
0.2
CaO
14
13
12
11
10
MgO
10
8
6
4
2
FeOT
23
22
21
20
19
18
17
16
Al2O3
15
13
11
9
7
TiO2
6
5
4
3
2
SiO2
49
48
47
46
45
44
P2O5
0.6
0.4
0.2
0
1200
1150
1100
1050
1000
Wt.% Oxide
Temperature °C

Figure 5

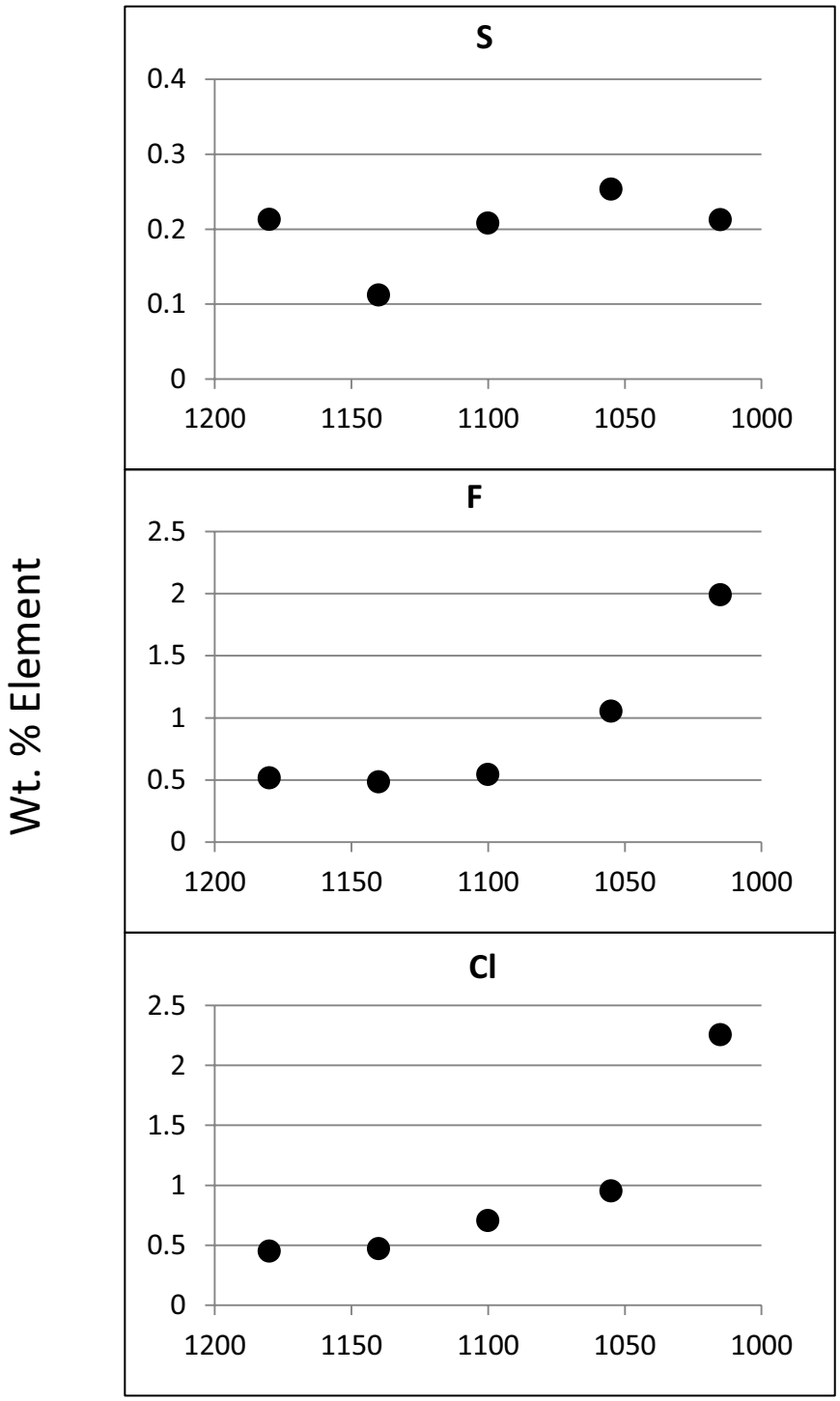
S
0.4
0.3
0.2
0.1
0
1200
1150
1100
1050
1000
F
2.5
2
1.5
1
0.5
0
1200
1150
1100
1050
1000
Cl
2.5
2
1.5
1
0.5
0
1200
1150
1100
1050
1000
Wt. % Element
Temperature °C

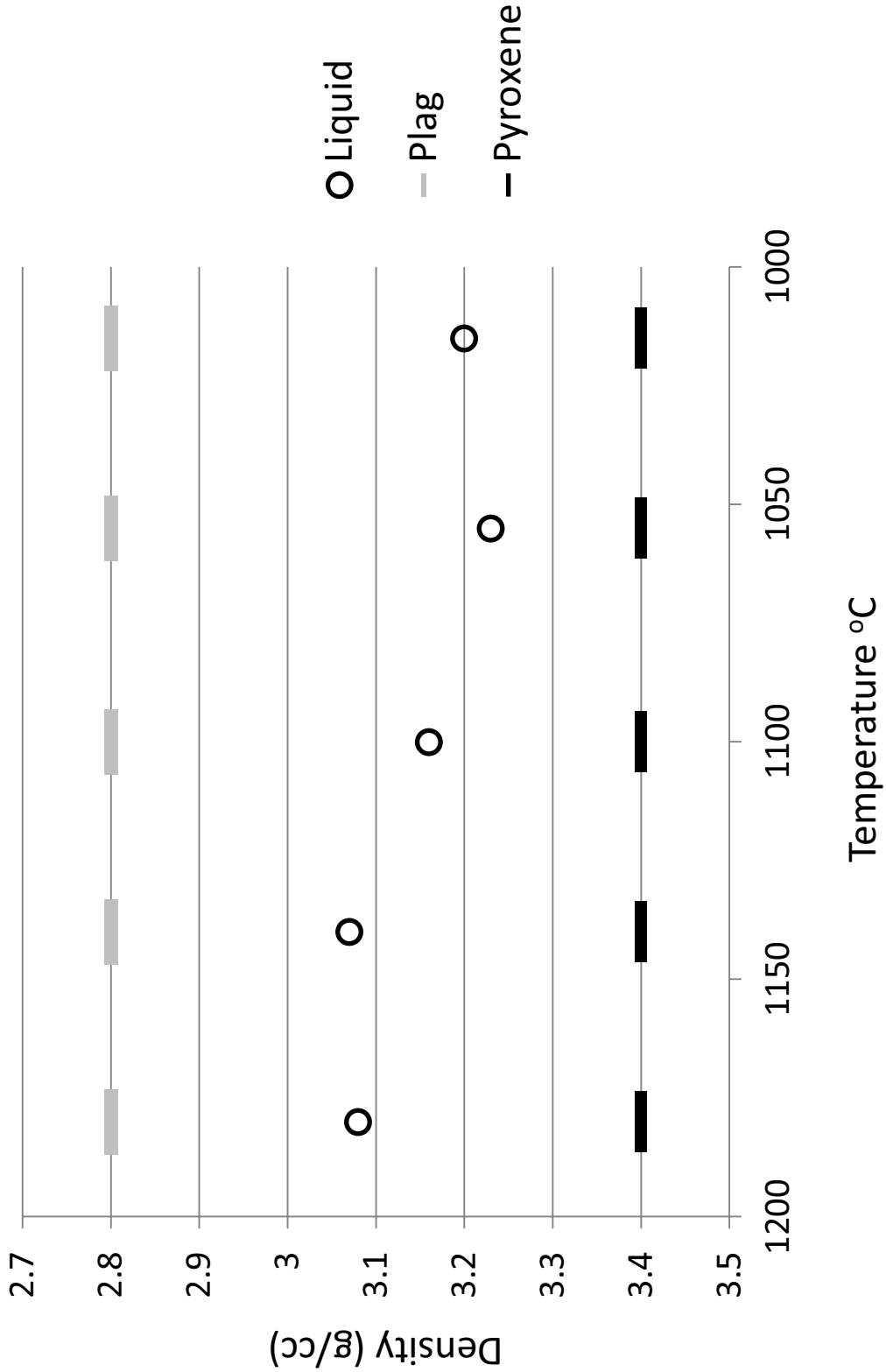
Liquid
Plag
Pyroxene
Density (g/cc)
2.7
2.8
2.9
3
3.1
3.2
3.3
3.4
3.5
1200
1150
1100
1050
1000
Temperature °C

Figure 6

Sample	1055°C	15388	12054	12047
SiO2	46.86	44.20	45.86	45.30
TiO2	5.47	5.91	4.63	5.20
Al2O3	9.64	11.10	10.47	10.10
FeO	21.15	19.10	19.50	20.50
MnO	0.27	0.35	0.29	0.29
MgO	4.05	8.00	6.67	6.59
CaO	11.65	10.20	11.93	11.32
Na2O	0.44	0.32	0.31	0.31
K2O	0.22	-	0.07	0.08
P2O5	0.25	0.06	0.06	0.08

Table 3